frontiers | Frontiers in Materials

TYPE Mini Review
PUBLISHED 22 August 2025
DOI 10.3389/fmats.2025.1612166

OPEN ACCESS

EDITED BY
Jing Zhou,
Chinese Academy of Sciences (CAS), China

REVIEWED BY
Kosuke Sugawa,
Nihon University, Japan

*CORRESPONDENCE
Junyoung Kwon,
jkwon@pknu.ac.kr

†These authors have contributed equally to this work and share first authorship

RECEIVED 15 April 2025
ACCEPTED 28 July 2025
PUBLISHED 22 August 2025

CITATION
Hong J, Choi Y and Kwon J (2025) Hierarchically self-assembled semiconducting and polysaccharide nanocrystals with multiscale chirality.
Front. Mater. 12:1612166.
doi: 10.3389/fmats.2025.1612166

Hierarchically self-assembled semiconducting and polysaccharide nanocrystals with multiscale chirality

Jai Hong†, Yujeong Choi† and Junyoung Kwon*

Major of Nanotechnology Engineering, Pukyong National University, Busan, Republic of Korea

Hierarchically chiral structures exhibit multiscale chirality across multiple length scales, ranging from the atomic to the micrometer scale. Recent studies have investigated their pronounced circular dichroism (CD) signals, chemical stability, and new properties, demonstrating their potential for diverse applications. This review focuses on the characteristics of semiconductor and polysaccharide nanocrystals that exhibit hierarchical architectures with two or more levels, with structural features ranging from 0.1 nm to 10 nm, 1 μm, and up to 10 μm. Particular attention is paid to small nanoparticles such as Cu_2S and CdTe in the category of semiconductors, and to cellulose and chitin nanocrystals among organic nanocrystals. Chiral semiconducting nanocrystals exhibit distinctive characteristics, including remarkable self-assembly capabilities into hierarchical structures and corresponding optical activities. Polysaccharide nanocrystals such as cellulose nanocrystals can be self-assembled into a chiral nematic liquid crystal phase, exhibiting strong chiral light reflection. This review provides a brief overview of recent studies of hierarchically chiral nanomaterials and their potential applications in optoelectronic devices, tunable color films, and optical sensors. This will facilitate a deeper understanding of underlying mechanisms and functional properties of hierarchically self-assembled chiral nanomaterials.

KEYWORDS

chiral, self-assembly, semiconductor, polysaccharide nanocrystals, multiscale chiral, hierarchical, chiroptical activity, nanostructures

1 Introduction

Chirality refers to a geometric property in which an object exists as a non-superimposable mirror image, like left and right hands (Lebreton et al., 2018). In contrast, achiral objects are identical to their mirror images. Chirality is widely observed in nature, and in particular, specific chiral forms are selectively preferred in biomolecules. Introducing chirality into materials imparts unique optical, electronic, and magnetic properties that distinguish them from their achiral counterparts. These properties include circular dichroism (CD), differences in light reflection, emission, transmission, and electron spin selectivity (Ray et al., 2006; Ray et al., 1999). Various strategies have been developed for the synthesis of chiral nanomaterials, including

templating methods (Guerrero-Martínez et al., 2011; McPeak et al., 2014; Yeom et al., 2013), assembling achiral nanoparticles into chiral structures (Mastroianni et al., 2009; Yan et al., 2012; Kuzyk et al., 2012), the use of chiral capping agents (Moloney et al., 2015; Ben-Moshe et al., 2014; Park et al., 2021), and synthesis using circularly polarized light (Yeom et al., 2015). Through these approaches, chirality can be introduced into materials, giving rise to novel electronic, optical, and magnetic properties not previously observed. As a result, research in this field has been actively progressing.

Chiral nanomaterials can be even more functional when hierarchically self-assembled, possessing multiscale chirality ranging from the atomic to micrometer scales (Figure 1A). Since the physicochemical and structural characteristics of nanomaterials are size-dependent, one can design nanostructures with more tailored functionalities by engineering chirality in multiscale domain that transcend specific length scales. Thus, there have been significant efforts to the design and fabrication of hierarchically chiral structures. This review investigates particularly semiconducting and polysaccharide nanocrystals as building blocks for fabrication of hierarchically chiral structures, with an emphasis on elucidating their structural and optical properties. Furthermore, representative applications of hierarchically chiral structures in optics, sensing, and electronics are presented. Note that materials such as metal-organic frameworks (MOFs) and perovskites, which do not meet these specific criteria of intermediate chiral form of nanocrystal, have been excluded from the scope of discussion.

2 Hierarchically chiral semiconducting materials

Semiconducting and metal nanomaterials have non-trivial long-range attraction (London dispersion attraction) compared to ceramic nanomaterials, thus effectively self-organized to form chiral microstructures (Án and gyán, 2020). For example, cysteine (Cys)-capped Cu_2S nanoparticles (NPs) can be self-assembled into microstructures exhibiting chirality from the nanoscale to the microscale (Park et al., 2021). The chirality transfer from molecular to micro-level was investigated to be governed by the interplay between interparticle attractive and repulsive forces (Xia et al., 2011). Immediately after synthesis, an excess of Cys ligands passivated the NP surfaces, ensuring colloidal stability (Figure 1B). Over time of incubation (1 h), short-range attractive interactions were enhanced leading to the formation of supraparticles (SPs) with diameters ranging from 10 to 40 nm (Tang et al., 2002). After 2 h, intermediate pearl-necklace-like assemblies appeared. By 5 h, these SPs reorganized primarily at the termini and edges to form nanoleaves (NLs) (Figure 1C). By 10 h, NLs were extensively formed (Park et al., 2021) and as electrostatic repulsion was further minimized these NLs underwent hierarchical stacking, culminating in the formation of nanoflowers (NFs) after 20 h (Figure 1D). This sequential self-assembly represents a pivotal mechanism for hierarchical chirality transfer, ultimately yielding well-defined microscale chiral architectures. To elucidate the stepwise chirality transfer during self-assembly, circular dichroism (CD) spectroscopy was employed. At the early stage (2 h), the formation of SPs and pearl-necklace-like structures led to an increase in CD signal intensity at 213 nm and 249 nm (Figure 1G). As the assembly evolved into NLs, new CD peaks emerged at 300 nm and 650 nm, albeit with weak intensity. After 10 h of aging, the CD peaks redshifted from 249 nm to 300 nm–263 nm and 365 nm, respectively, due to the formation of NLs. With further assembly, NFs became dominant, showing intensified CD responses at 365 nm and 650 nm. These results strongly support the successful transfer of molecular chirality from Cys to the nanoscale chirality of the NPs (Park et al., 2021). Subsequently, the NPs acted as chiral building blocks, driving a stepwise hierarchical assembly process that ultimately enabled chirality transfer to the microscale (Park et al., 2021).

Apart from Cu2S NPs, CdTe NPs also exhibit self-assembly behavior resulting in optically active helical structures (Yan et al., 2019). This process is primarily driven by strong face-to-face interactions between NPs, maximizing coordination and hydrogen bonding (Yan et al., 2019). Similar to other nanostructures, CdTe NPs experience electrostatic repulsion due to surface charges, which balances the attractive forces during self-assembly. The resulting continuous tetrahedral-based helices correspond to the Boerdijk–Coxeter–Bernal (BCB) model (Figures 1E,F). Previous studies have reported that BCB helices formed from NPs typically appear as racemic mixtures (Fejer et al., 2014; Fernández et al., 2015; Nagaoka et al., 2018). However, in this study, 100% enantiopure helices were successfully obtained. This selective assembly into single-handed helices arises from relative angular displacement between neighboring NPs, governed by collective interactions among the chiral surface ligands. The geometrical parameters of the helices can be modulated by controlling Cd^{2+} concentration, pH, and surface ligand composition. However, since these parameters also significantly impact assembly yield, identifying the factors that selectively influence the helical pitch rather than overall yield is critical (Yan et al., 2019). The geometric parameters of the helix can be tuned by adjusting the Cd^{2+} ion concentration, pH level, and surface ligand composition. However, as these parameters also significantly affect the assembly yield, identifying the factors that influence the helix pitch is more critical than maximizing overall yield. During the self-assembly of CdTe nanoparticles (NPs), it was found that the interparticle coordination strength can be effectively modulated by controlling the volume ratio of water (V^{H2O}) to methanol (V^{MeOH}) (Figure 1H). Furthermore, varying the V^{H2O}:V^{MeOH} ratio led to the formation of diverse assembly morphologies. At a V^{H2O}:V^{MeOH} ratio of 1:1, spherical CdS and block-like Te structures were observed, while a 1:2 ratio resulted in fibrous structures. When the ratio was increased to 1:3, characteristic helical structures were formed. The helical pitch increased from 539 ± 82 nm at 1:3 to 940 ± 103 nm at 1:5, corresponding to a redshift in CD peaks (Yan et al., 2019). This study elucidates the critical role of surface ligand density, coordination bonding strength, and solvent environment in governing the chiral self-assembly of CdTe nanoparticles (CdTe NPs) via circular dichroism (CD) spectral analysis (Figure 1I). The self-assembly behavior exhibited a non-linear dependence on L-Cys concentration, with well-defined helical structures predominantly forming in the 5–15 mM range. In both aqueous and mixed solvent systems, nanohelices of several micrometers in size were formed, exhibiting right-handed or left-handed chirality depending on the use of L- or D-Cys, respectively. The resulting structures displayed strong optical activity across the 200–800 nm range, with additional CD signals observed in the

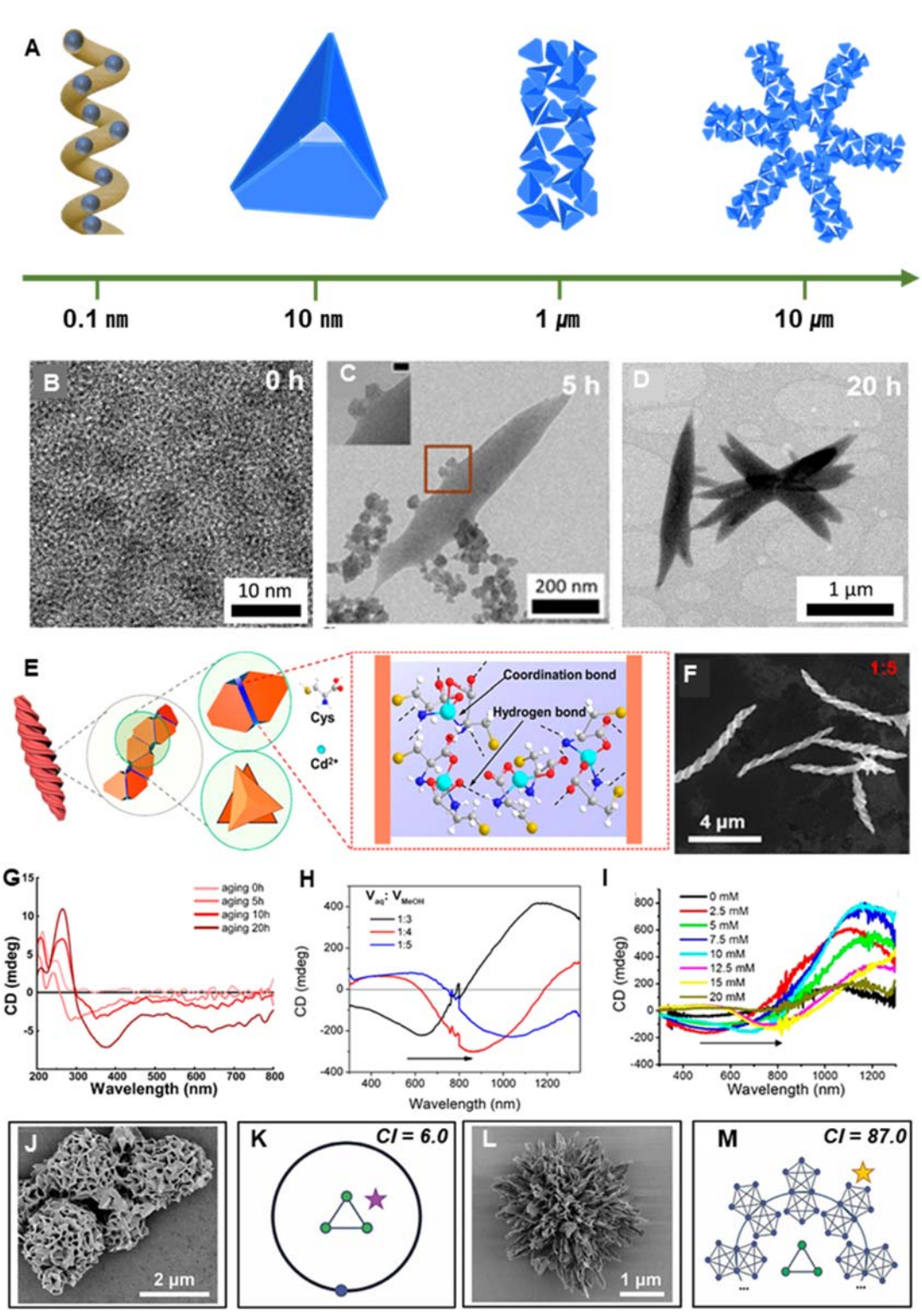

FIGURE 1
Semiconductor/Metal-originated semiconductor. **(A)** Chiral hierarchical structures form across multiple scales: from atomic-level chirality (~0.1 nm), to molecular (~10 nm), rod-like (~1 μm), and finally multi-rod assemblies (~10 μm), each step exhibiting chiral organization. **(B)** TEM image of *L*-Cys-Cu_2S NP at 0 h **(C)** TEM image of *L*-Cys-Cu_2S NL at 5 h **(D)** TEM image of *L*-Cys-Cu_2S NF at 20 h. **(E)** Assembly process of CdTe NPs into helical structures. **(F)** SEM image of CdTe helical structures formed with a V_{aq}:V_{MeOH} ratio of 1:5. **(G)** CD data at different aging times (0h, 5h, 10h, 20h). **(B–F)** reprinted with permission from (Park et al., 2021). Copyright 2021 American Chemical Society. **(H)** CD spectrum representing the chiral optical properties of the structure formed in F. **(I)** CD spectra showing the effect of varying *L*-Cys concentrations (0, 2.5, 5, 10, 12.5, 15, 20 mM). **(E,F,H,I)** reprinted with permission from (Yan et al., 2019). Copyright 2019 American Chemical Society. **(J)** SEM image of achiral supraparticle Au-thiolate. **(K)** Complexity index (CI) and GT model of J. **(L)** SEM image of Au–*L*-Cys CLIP. **(M)** CI and graph theory (GT) model of L. **(J–M)** reprinted with permission from (Jiang et al., 2020). Copyright 2020 The American Association for the Advancement of Science.

200–350 nm region, attributed to coordination interactions between Cd2+ ions and Cys ligands. These findings highlight the importance of precise control over assembly parameters for the rational design of chiral nanomaterials (Yan et al., 2019).

Particles found in biological systems often exhibit spiky, twisted, reticulated, or fractal morphologies and incorporate nanoscale structural elements. These particles can be classified as hierarchically organized particles (HOPs) due to their multiscale architecture. Notably, understanding how chirality governs the assembly patterns of structural units of varying sizes holds substantial academic significance. Gold exhibit metallic properties; however, when their size is reduced to 1–2 nm or smaller, a bandgap is formed, causing them to exhibit semiconductor characteristics. Recent studies have experimentally demonstrated that chirality can be preserved across nanoscale, mesoscale, and macroscale levels using semiconductor-based systems. At the nanoscale, individual gold-cysteine (Au-*L*-Cys) nanoparticles exhibit chirality, while at the mesoscale, these nanoparticles form helical nanoribbon structures (Jiang et al., 2020). At the macroscale, these nanoribbons further organize into radially spiky coccolith-like particles (CLIPs) (Figure 1L) or kayak-shaped particles (Jiang et al., 2020). Ultrasonic fragmentation (sonication) of HOPs into individual nanoribbons revealed that nanoribbons exhibit right-handed twisting at the nanoscale, while they adopt left-handed helicity at the mesoscale (Jiang et al., 2020). This provides experimental evidence that chirality can be inverted across hierarchical scales. The nanoribbons further assembled into complex radial architectures, closely resembling the skeletal formations of coccolithophores (Figure 1L). These structural transformations were accompanied by increased CD signals in both the ultraviolet-visible and infrared spectral regions (Jiang et al., 2020). Generally, polydisperse nanoparticles have a higher tendency to form disordered structures (Grason, 2016; Gibaud et al., 2012; Gao et al., 2019). However, this study demonstrated that size-diverse particles can instead assemble into highly ordered hierarchical chiral structures (Jiang et al., 2020). This suggests that intermolecular interactions, such as electrostatic forces (Xia et al., 2011; Grason, 2016; Gibaud et al., 2012) and chiral-induced binding, play a more critical role than particle size. Using graph theory (GT) to evaluate structural complexity, the Complexity Index (CI) values for various HOPs including reticulated supraparticles, kayak particles, and CLIPs ranged from 6.0 to 87.0 (Figures 1J–M). In contrast, previously reported NP assemblies had CI values between 1.5 and 38.25, indicating that CLIPs exceed the complexity of naturally occurring coccolithophores. This supports the notion that increasing chirality enhances structural complexity and promotes ordered self-assembly. The circular dichroism spectrum of CLIPs displayed nearly perfect mirror symmetry with sharp peaks at 250, 310, 350, and 380 nm, which matched the electronic transitions calculated for Au-*L*-Cys nanoplate models. Upon disassembly into stacked nanoribbons, peaks at 420, 560, and 830 nm disappeared, indicating that these features are unique to fully assembled CLIPs. The assembled state and morphology of HOPs significantly influenced light scattering contributions, thereby altering the sign of the circularly polarized light emission (CPLE) spectra (Jiang et al., 2020). CLIPs showed positive CPLE peaks, while disassembled nanoribbons exhibited negative values, attributed to differential scattering. CD peaks between 500 and 1200 nm vanished upon disassembly, and CPLE plots showed vertical symmetry across the central axis, highlighting the distinctive optical properties of CLIPs These findings align with electrodynamics simulations and support the fundamental physical mechanisms underlying the hierarchical evolution of nanoscale systems into HOPs. In conclusion, the preservation of chirality across multiple scales enhances both CD and CPLE responses, indicating that nanoscale chirality is not an isolated phenomenon but one that integrates into higher-order architectures. The discovery of multi-scale chirality presents significant potential for applications in optical sensing, nanophotonics, chiral catalysis, and bioinspired materials (Jiang et al., 2020).

3 Hierarchically chiral polysaccharide materials

Cellulose and chitin are representative organic materials with hierarchically chiral structures and have emerged as promising bio-based colloids attracting significant interest as environmentally friendly and sustainable functional materials (Bai et al., 2020). In particular, cellulose demonstrates remarkable self-assembly capabilities that lead to the formation of a chiral nematic (cholesteric) liquid crystal phase extensively investigated for its tunable reflective color depending on pitch length. Although chitin exhibits a similar cholesteric phase, its application as an optical material remains underdeveloped (Narkevicius et al., 2022).

Cellulose is found in plants, fruits (Vignolini et al., 2016), and other related sources. In nature, it exists in the form of nanofibrils, where β-1,4-glycosidic polymer chains are tightly bundled together (Figure 2A). Cellulose nanofibers (CNFs) consist of both crystalline and amorphous regions. The amorphous domains can be selectively removed via sulfuric acid hydrolysis, resulting in rod-shaped nanoparticles composed solely of crystalline cellulose, known as cellulose nanocrystals (CNCs) (Figure 2B). (Vignolini et al., 2016; Schütz et al., 2020; Pan et al., 2010) As the concentration of CNCs increases, phase separation occurs, and the rod-like particles spontaneously align along a preferred direction (director, n), forming a nematic liquid crystal phase. Long-range orientational correlations in the nematic phase induce a helical distortion in the director field, n(r), which undergoes periodic rotation around a specific axis, known as the helical axis (m), resulting in a helicoidal structure (Figure 2C). (Schütz et al., 2020) Upon drying the CNC suspension, an optical film that retains the cholesteric phase can be fabricated (Pan et al., 2010; Parker et al., 2018; Frka-Petesic et al., 2023).

Chitin, similar to cellulose, can be extracted from the exoskeletons of crustaceans and insects as well as from fungi. Chitin nanocrystals (ChNCs) are typically obtained through a series of treatments including HCl and NaOH processing, decolorization, and acid hydrolysis with HCl. ChNCs can self-assemble into cholesteric liquid crystalline phases; however, their visible light reflection is less pronounced compared to that of CNC films. This aspect is further discussed in relation to their optical properties (Bai et al., 2020; Narkevicius et al., 2022; Narkevicius et al., 2019).

Organic materials form hierarchical chiral structures through self-assembly, driven by chiral interactions between nanorods (Parker et al., 2018). As the suspension dries, the nanorods move closer together, leading to a decrease in pitch and an enhancement of chiral interactions, ultimately resulting in the formation of

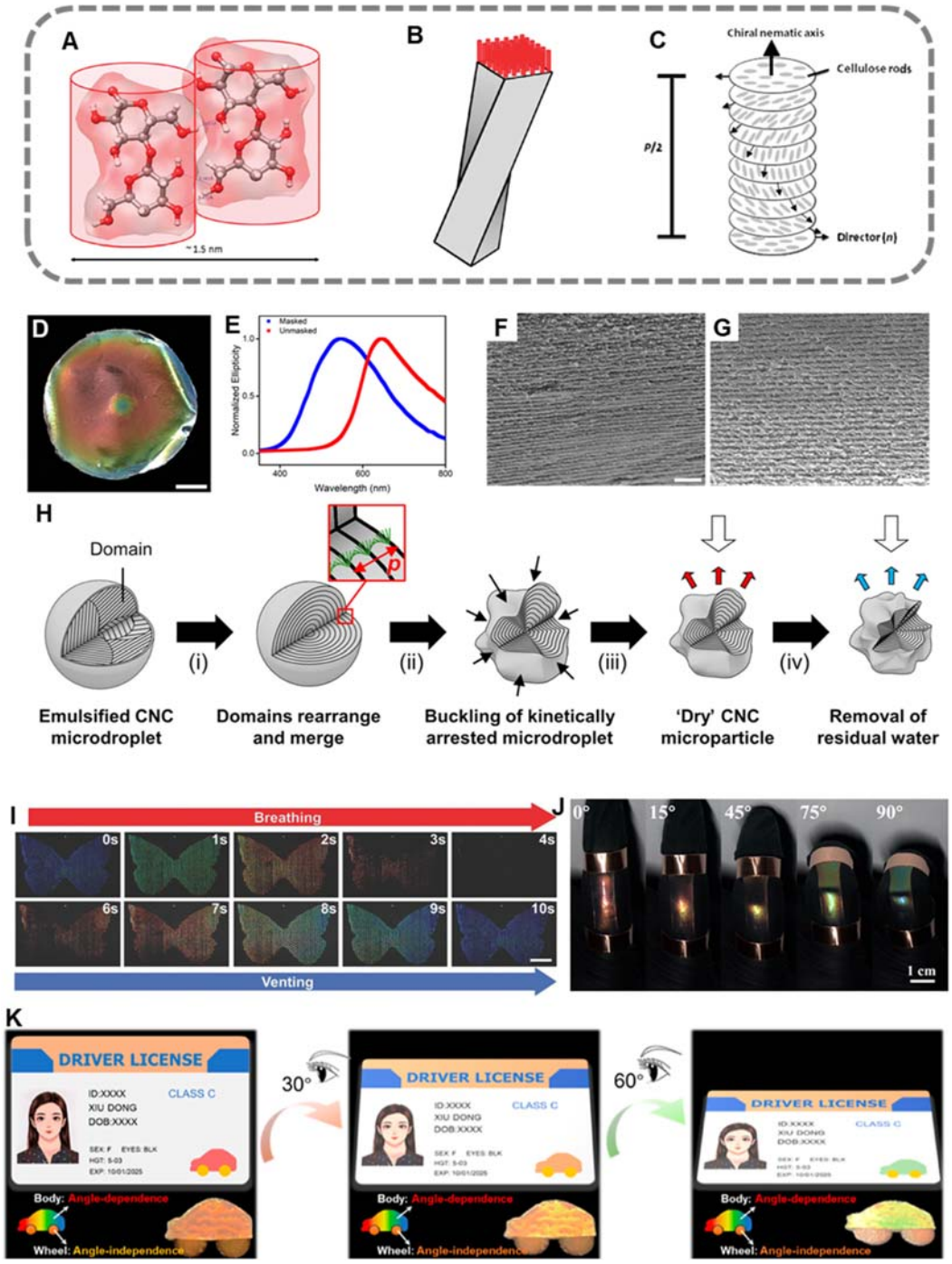

FIGURE 2
Structural and Optical Characteristics of Hierarchical Chiral Organic Materials **(A)** Schematic representation of CNF in a polymer chain form. **(B)** Illustration of a helical rod-like CNC structure composed of nine CNFs. **(C)** Depiction of the formation of a cholesteric phase, where individual rod-like CNCs assemble into layered structures. **(A–C)** reprinted with permission from (Pan et al., 2010). Copyright 2010 American Chemical Society. **(D)** Optical gradient implementation within a single CNC film using a cellulose acetate mask and **(E)** corresponding CD analysis. **(F)** SEM image of the rapidly evaporated CNC film, showing an increased pitch. **(G)** SEM image of the slowly evaporated CNC film, showing a decreased pitch. **(D–G)** reprinted with permission from (Tran et al., 2018). Copyright 2018 American Chemical Society. **(H)** Schematic illustration of CNC-based micro-particles fabricated via an emulsion-based process. Reproduced with permission from ref (Parker et al., 2022) under CC-BY. Copyright 2022 The Authors. Applications Based on the Optical Properties of Organic Materials. **(I)** A photograph of CNC microfilms deposited on a patterned glass substrate, demonstrating a blue "butterfly" dot matrix that rapidly changes color within a few seconds in response to moisture from exhaled breath. Reproduced under terms of the CC-BY license (Zhao et al., 2019). Copyright 2019, The Authors. **(J)** A series of photographs illustrating the color variation of FIL–CNC nanostructured films at different finger bending angles of 0°, 15°, 45°, 75°, and 90°. Reprinted with permission from (Li et al., 2023). Copyright 2023 American Chemical Society. **(K)** A schematic illustration and corresponding local photographs of an anti-counterfeiting driver's license utilizing CNC/Gly and CNC/Gly/PDDA films, demonstrating color variation at different viewing angles. Reprinted with permission from (Dong et al., 2022). Copyright 2022 American Chemical Society.

a structurally colored film with distinctive optical properties. Structural color arises from the interaction between a material's nanostructure and light, producing specific colors. Unlike dyes or pigments, which absorb specific wavelengths, structural color emerges from optical interference effects. This phenomenon is commonly observed in nature, such as in the exocarp of certain fruits or the exoskeletons of insects. It is generated when organic materials adopt a helical arrangement and can also be artificially reproduced by controlling the nanostructure in engineered films. Structural color offers significant advantages over conventional dyes or pigments, as it does not fade over time and exhibits a reflectance that is over ten times stronger (Narkevicius et al., 2022; Frka-Petesic et al., 2023; Abbasi Moud, 2022).

For structural color to emerge, the pitch in the cholesteric structure plays a crucial role. The pitch (p) refers to the distance between two nanorods that have completed a full 360° rotation around the helical axis (m) and are aligned in the same direction. According to Bragg's law, when incident light interacts with a CNC film, the wavelength of the reflected light—and consequently the perceived color—depends on the pitch and the orientation of the helical axis relative to the film normal. The reflected wavelength (λ) is defined by the Bragg equation:

$$\lambda = nP \sin(\theta)$$

where λ is the reflected wavelength, P is the helical pitch, θ is the angle of incidence, and n is the average refractive index of the material. When the incident light is perpendicular to the crystal plane ($\sin(\theta) = 1$), the equation simplifies to $\lambda = nP$ (Abbasi Moud, 2022). When the pitch corresponds to wavelengths within the visible spectrum (400–700 nm), constructive interference occurs, leading to the strong reflection of specific colors. To achieve this effect, the pitch must be tuned within the range of 250–450 nm. Numerous studies have reported that pitch is influenced by various factors, including additives, concentration, ionic strength, pH, temperature, humidity, evaporation rate, magnetic fields, and electric fields (Parker et al., 2018; Frka-Petesic et al., 2023; Narkevicius et al., 2019). This level of control applies similarly to cellulose and chitin-based systems.

Tran et al. controlled the evaporation rate to achieve tunable structural colors. In their study, red structural coloration was observed in CNC films dried over the course of 1 day, whereas blue coloration appeared in films dried over 10 days. This difference in drying time was utilized to perform a gradient evaporation experiment, successfully yielding an optical gradient within a single CNC film (Figure 2D). Circular dichroism (CD) spectroscopy revealed a decrease in reflection wavelength in the blue region of the film (Figure 2E). Scanning electron microscopy (SEM) analysis showed that the red-colored region exhibited a larger pitch (Figure 2F), while the blue-colored region displayed a smaller pitch (Figure 2G). (Tran et al., 2018) These results provide direct evidence for the correlation between helical pitch and structural color.

Controlling birefringence is also a key factor in enhancing the intensity of structural color. Birefringence refers to the phenomenon where light propagating in different directions within a material experience distinct refractive indices. A higher birefringence leads to an increase in reflectance (Frka-Petesic et al., 2023). This explains why CNC exhibits more pronounced visible reflection compared to ChNC. Due to its high birefringence, CNC can generate strong structural color, whereas ChNC has relatively lower birefringence. In fact, the minimum pitch observed in artificial chitin (ChNC) films has been reported to be approximately 650 nm, with no structural color observed in the visible spectrum (Narkevicius et al., 2019). However, Narkevicius, A., et al. successfully demonstrated visible light reflection by employing ChNCs with a short pitch of 360 ± 90 nm. Nevertheless, the resulting structural color was faint due to low reflectance. To overcome this limitation, intrinsic birefringence was enhanced via alkaline treatment, leading to more than a 100-fold increase in reflected color intensity (Narkevicius et al., 2022).

CNCs can exhibit structural coloration not only in film form but also as microparticles. Parker, R. M., et al. achieved structural coloration in microparticles by utilizing an emulsion-based process combined with the "buckling phenomenon." In their method, an aqueous CNC suspension is emulsified within hexadecane using a microfluidic flow-focusing device, generating fine droplets. Upon drying, the microdroplets kinetically arrest and undergo surface contraction, inducing buckling, which results in visible light reflection and the manifestation of structural color. The dried CNC microparticles initially exhibit a red-reflecting structural color. Through solvent or thermal treatment, additional contraction can be induced, causing a blue shift in the reflected color, ultimately allowing for the fabrication of red, green, and blue photonic microparticles (Figure L) (Parker et al., 2022).

The optical properties of organic materials can be utilized in various applications. Zhao, T. H. et al. developed a CNC film-based sensor that exhibits color changes in response to humidity variations. As humidity increases, the pitch expands, shifting the reflected color toward red; when humidity decreases, the pitch contracts, restoring the original blue color. This color transition occurs within one second (Figure 2I), demonstrating real-time responsiveness. Such characteristics highlight the potential for applications in environmental sensors, including smart windows, humidity control systems, and indoor air quality monitoring devices (Zhao et al., 2019).

Li, X. et al. developed an artificial skin with integrated optical and conductive properties. Infiltration of ionic liquids into CNC films enabled the fabrication of a bioinspired mechanochromic film with excellent ionic conductivity. Utilizing the principle that stretching the film reduces the pitch and induces a blue shift, a wearable sensor capable of detecting finger movements in real time was demonstrated (Figure 2J) (Li et al., 2023).

Dong, X. et al. developed a structurally colored CNC film with reduced angular dependence and an expanded color gamut by incorporating cationic poly (dimethyl diallyl ammonium chloride) (PDDA) and glycerol (Gly) to modulate the self-assembly behavior and helical pitch of CNCs. This advancement offers enhanced optical performance for applications such as anti-counterfeiting and smart coatings (Figure 2K) (Dong et al., 2022).

4 Concluding remarks

This review discusses the properties of multiscale materials based on their origin and structure, ultimately highlighting their pronounced chiral characteristics and unique optical behaviors. Fluorescent gold-originated microstructures exhibit enhanced

chirality, alongside increased structural complexity with a final CI value of 87.0. Size-dependent inversion of the CPLE signal suggests that the CLIP architecture plays a critical role in determining the optical properties in building blocks and organized particles. In semiconductor-originated nanostructures, morphological transitions from SP to NL and NF were observed depending on reaction time, accompanied by a gradual oxidation from Cu(I) to Cu(II). These changes resulted in the emergence of new peaks or amplification of existing signals in CD spectra. The retention of multiscale chirality in semiconductor-based materials holds great promise for applications in optical sensors, nanophotonic devices, chiral catalysis, and biomimetic materials. Organic nanocrystals such as nanoscale CNCs and ChNCs undergo self-assembly to form helical pitches, enabling the fabrication of optical films and structural color pigments. Due to their pitch-dependent structural coloration, extensive research is being conducted to tune the pitch and thereby control the optical appearance. In particular, CNCs exhibit distinctive optical properties that can be applied to optical sensors, wearable devices, and anti-counterfeiting technologies. However, ChNCs possess relatively low birefringence, which limits their applicability in certain areas, representing an ongoing challenge for future research. In future studies, the development of hierarchically structured nanomaterials based on various material systems is expected to significantly broaden the application potential of this field. In particular, it would be highly intriguing and meaningful to investigate a bespoke control of chirality across different scales from molecular, nanometer to higher-order hierarchical architectures. Notably, such hierarchically chiral microstructures consisting of intermediate nanocrystal chirality have rarely been explored in material systems like MOFs and perovskites. Therefore, extending this research framework to include these classes of materials could offer novel insights and open up new possibilities. We believe that such efforts will contribute not only to advancing the fundamental understanding of chirality in nanostructures but also to enabling practical applications in areas such as optics, sensing, and catalysis.

Author contributions

JH: Investigation, Conceptualization, Writing – original draft. YC: Investigation, Writing – original draft, Conceptualization. JK: Writing – review and editing, Supervision.

Funding

The author(s) declare that financial support was received for the research and/or publication of this article. This work was supported by a Research Grant of Pukyong National University (2024).

Conflict of interest

The authors declare that the research was conducted in the absence of any commercial or financial relationships that could be construed as a potential conflict of interest.

Generative AI statement

The author(s) declare that no Generative AI was used in the creation of this manuscript.

Publisher's note

References

Abbasi Moud, A. (2022). Chiral liquid crystalline properties of cellulose nanocrystals: fundamentals and applications. *ACS omega* 7 (35), 30673–30699. doi:10.1021/acsomega.2c03311

Ángyán, J., Dobson, J., Jansen, D., and Gould, T. (2020). *Introduction, in london dispersion forces in molecules, solids and nano-structures: an introduction to physical models and computational methods*. Royal Society of Chemistry. doi:10.1039/9781782623861-00001

Bai, L., Kämäräinen, T., Xiang, W., Majoinen, J., Seitsonen, J., Grande, R., et al. (2020). Chirality from cryo-electron tomograms of nanocrystals obtained by lateral disassembly and surface etching of never-dried chitin. *ACS nano* 14 (6), 6921–6930. doi:10.1021/acsnano.0c01327

Ben-Moshe, A., Wolf, S. G., Sadan, M. B., Houben, L., Fan, Z., Govorov, A. O., et al. (2014). Enantioselective control of lattice and shape chirality in inorganic nanostructures using chiral biomolecules. *Nat. Commun.* 5 (1), 4302. doi:10.1038/ncomms5302

Dong, X., Wu, J. M., Zhang, Z. L., Wang, Z. L., Song, F., et al. (2022). Non-iridescent and wide-color-range structural coloration enabled by cellulose nanocrystals with a controlled long-range photonic structure and helical pitch. *ACS Sustain. Chem. and Eng.* 10 (32), 10641–10648. doi:10.1021/acssuschemeng.2c02501

Fejer, S. N., Chakrabarti, D., Kusumaatmaja, H., and Wales, D. J. (2014). Design principles for bernal spirals and helices with tunable pitch. *Nanoscale* 6 (16), 9448–9456. doi:10.1039/c4nr00324a

Fernández, M. S., Misko, V., and Peeters, F. (2015). Self-assembly of janus particles into helices with tunable pitch. *Phys. Rev. E* 92 (4), 042309. doi:10.1103/physreve.92.042309

Frka-Petesic, B., Parton, T. G., Honorato-Rios, C., Narkevicius, A., Ballu, K., Shen, Q., et al. (2023). Structural color from cellulose nanocrystals or chitin nanocrystals: self-assembly, optics, and applications. *Chem. Rev.* 123 (23), 12595–12756. doi:10.1021/acs.chemrev.2c00836

Gao, C., Kewalramani, S., Valencia, D. M., Li, H., McCourt, J. M., Olvera de la Cruz, M., et al. (2019). Electrostatic shape control of a charged molecular membrane from ribbon to scroll. *Proc. Natl. Acad. Sci.* 116 (44), 22030–22036. doi:10.1073/pnas.1913632116

Gibaud, T., Barry, E., Zakhary, M. J., Henglin, M., Ward, A., Yang, Y., et al. (2012). Reconfigurable self-assembly through chiral control of interfacial tension. *Nature* 481 (7381), 348–351. doi:10.1038/nature10769

Grason, G. M. (2016). Perspective: geometrically frustrated assemblies. *J. Chem. Phys.* 145 (11). doi:10.1063/1.4962629

Guerrero-Martínez, A., Auguié, B., Alonso-Gómez, J. L., Džolić, Z., Gómez-Graña, S., Žinić, M., et al. (2011). Intense optical activity from three-dimensional chiral ordering of plasmonic nanoantennas. *Angew. Chem. Int. Ed.* 50 (24), 5499–5503. doi:10.1002/anie.201007536

Jiang, W., Qu, Z. b., Kumar, P., Vecchio, D., Wang, Y., Ma, Y., et al. (2020). Emergence of complexity in hierarchically organized chiral particles. *Science* 368 (6491), 642–648. doi:10.1126/science.aaz7949

Kuzyk, A., Schreiber, R., Fan, Z., Pardatscher, G., Roller, E. M., Högele, A., et al. (2012). DNA-Based self-assembly of chiral plasmonic nanostructures with tailored optical response. *Nature* 483 (7389), 311–314. doi:10.1038/nature10889

Lebreton, G., Géminard, C., Lapraz, F., Pyrpassopoulos, S., Cerezo, D., Spéder, P., et al. (2018). Molecular to organismal chirality is induced by the conserved myosin 1D. *Science* 362 (6417), 949–952. doi:10.1126/science.aat8642

Li, X., Yang, Y., Valenzuela, C., Zhang, X., Xue, P., Liu, Y., et al. (2023). Mechanochromic and conductive chiral nematic nanostructured film for bioinspired ionic skins. *ACS nano* 17 (13), 12829–12841. doi:10.1021/acsnano.3c04199

Mastroianni, A. J., Claridge, S. A., and Alivisatos, A. P. (2009). Pyramidal and chiral groupings of gold nanocrystals assembled using DNA scaffolds. *J. Am. Chem. Soc.* 131 (24), 8455–8459. doi:10.1021/ja808570g

McPeak, K. M., van Engers, C. D., Blome, M., Park, J. H., Burger, S., Gosálvez, M. A., et al. (2014). Complex chiral colloids and surfaces *via* high-index off-cut silicon. *Nano Lett.* 14 (5), 2934–2940. doi:10.1021/nl501032j

Moloney, M. P., Govan, J., Loudon, A., Mukhina, M., and Gun'ko, Y. K. (2015). Preparation of chiral quantum dots. *Nat. Protoc.* 10 (4), 558–573. doi:10.1038/nprot.2015.028

Nagaoka, Y., Tan, R., Li, R., Zhu, H., Eggert, D., Wu, Y. A., et al. (2018). Superstructures generated from truncated tetrahedral quantum dots. *Nature* 561 (7723), 378–382. doi:10.1038/s41586-018-0512-5

Narkevicius, A., Steiner, L. M., Parker, R. M., Ogawa, Y., Frka-Petesic, B., and Vignolini, S. (2019). Controlling the self-assembly behavior of aqueous chitin nanocrystal suspensions. *Biomacromolecules* 20 (7), 2830–2838. doi:10.1021/acs.biomac.9b00589

Narkevicius, A., Parker, R. M., Ferrer-Orri, J., Parton, T. G., Lu, Z., van de Kerkhof, G. T., et al. (2022). Revealing the structural coloration of self-assembled chitin nanocrystal films. *Adv. Mater.* 34 (31), 2203300. doi:10.1002/adma.202203300

Pan, J., Hamad, W., and Straus, S. K. (2010). Parameters affecting the chiral nematic phase of nanocrystalline cellulose films. *Macromolecules* 43 (8), 3851–3858. doi:10.1021/ma902383k

Park, K. H., Kwon, J., Jeong, U., Kim, J. Y., Kotov, N. A., and Yeom, J. (2021). Broad chiroptical activity from ultraviolet to short-wave infrared by chirality transfer from molecular to micrometer scale. *ACS nano* 15 (9), 15229–15237. doi:10.1021/acsnano.1c05888

Parker, R. M., Guidetti, G., Williams, C. A., Zhao, T., Narkevicius, A., Vignolini, S., et al. (2018). The self-assembly of cellulose nanocrystals: hierarchical design of visual appearance. *Adv. Mater.* 30 (19), 1704477. doi:10.1002/adma.201704477

Parker, R. M., Zhao, T. H., Frka-Petesic, B., and Vignolini, S. (2022). Cellulose photonic pigments. *Nat. Commun.* 13 (1), 3378. doi:10.1038/s41467-022-31079-9

Ray, K., Ananthavel, S. P., Waldeck, D. H., and Naaman, R. (1999). Asymmetric scattering of polarized electrons by organized organic films of chiral molecules. *Science* 283 (5403), 814–816. doi:10.1126/science.283.5403.814

Ray, S., Daube, S. S., Leitus, G., Vager, Z., and Naaman, R. (2006). Chirality-induced spin-selective properties of self-assembled monolayers of DNA on gold. *Phys. Rev. Lett.* 96 (3), 036101. doi:10.1103/physrevlett.96.036101

Schütz, C., Bruckner, J. R., Honorato-Rios, C., Tosheva, Z., Anyfantakis, M., and Lagerwall, J. P. F. (2020). From equilibrium liquid crystal formation and kinetic arrest to photonic bandgap films using suspensions of cellulose nanocrystals. *Crystals* 10 (3), 199. doi:10.3390/cryst10030199

Tang, Z., Kotov, N. A., and Giersig, M. (2002). Spontaneous organization of single CdTe nanoparticles into luminescent nanowires. *Science* 297 (5579), 237–240. doi:10.1126/science.1072086

Tran, A., Hamad, W. Y., and MacLachlan, M. J. (2018). Fabrication of cellulose nanocrystal films through differential evaporation for patterned coatings. *ACS Appl. Nano Mater.* 1 (7), 3098–3104. doi:10.1021/acsanm.8b00947

Vignolini, S., Gregory, T., Kolle, M., Lethbridge, A., Moyroud, E., Steiner, U., et al. (2016). Structural colour from helicoidal cell-wall architecture in fruits of Margaritaria nobilis. *J. R. Soc. Interface* 13 (124), 20160645. doi:10.1098/rsif.2016.0645

Xia, Y., Nguyen, T. D., Yang, M., Lee, B., Santos, A., Podsiadlo, P., et al. (2011). Self-assembly of self-limiting monodisperse supraparticles from polydisperse nanoparticles. *Nat. Nanotechnol.* 6 (9), 580–587. doi:10.1038/nnano.2011.121

Yan, W., Xu, L., Xu, C., Ma, W., Kuang, H., Wang, L., et al. (2012). Self-assembly of chiral nanoparticle pyramids with strong R/S optical activity. *J. Am. Chem. Soc.* 134 (36), 15114–15121. doi:10.1021/ja3066336

Yan, J., Feng, W., Kim, J. Y., Lu, J., Kumar, P., Mu, Z., et al. (2019). Self-assembly of chiral nanoparticles into semiconductor helices with tunable near-infrared optical activity. *Chem. Mater.* 32 (1), 476–488. doi:10.1021/acs.chemmater.9b04143

Yeom, B., Zhang, H., Zhang, H., Park, J. I., Kim, K., Govorov, A. O., et al. (2013). Chiral plasmonic nanostructures on achiral nanopillars. *Nano Lett.* 13 (11), 5277–5283. doi:10.1021/nl402782d

Yeom, J., Yeom, B., Chan, H., Smith, K. W., Dominguez-Medina, S., Bahng, J., et al. (2015). Chiral templating of self-assembling nanostructures by circularly polarized light. *Nat. Mater.* 14 (1), 66–72. doi:10.1038/nmat4125

Zhao, T. H., Parker, R. M., Williams, C. A., Lim, K. T. P., Frka-Petesic, B., and Vignolini, S. (2019). Printing of responsive photonic cellulose nanocrystal microfilm arrays. *Adv. Funct. Mater.* 29 (21), 1804531. doi:10.1002/adfm.201804531